PCCP

Accepted Manuscript

ROYAL SOCIETY OF CHEMISTRY

www.rsc.org/pccp

How Does the Plasmonic Enhancement on Molecular Absorption Depend on the Energy Gap between Molecular Excitation and Plasmon Mode: A Mixed TDDFT/FDTD Investigation

Jin Sun[1], Guang Li[1] and WanZhen Liang[2,*]

[1] *School of Physics and Materials Science, Anhui University, Hefei 230601, People's Republic of China*

[2] *State Key Laboratory of Physical Chemistry of Solid Surfaces, Collaborative Innovation Center of Chemistry for Energy Materials, and Department of Chemistry, College of Chemistry and Chemical Engineering, Xiamen University, Xiamen 361005, People's Republic of China*

(Dated: May 28, 2015)

A real-time time-dependent density functional theory coupled with the classical electrodynamics finite difference time domain technique is employed to systematically investigate the optical properties of hybrid systems composed of silver nanoparticles (NPs) and organic adsorbates. The results demonstrate that the molecular absorption spectra throughout the whole energy range can be enhanced by the surface plasmon resonance of Ag NPs, however, the absorption enhancement ratio (AER) for each absorption band differs significantly with each other, leading to the quite different spectral profiles in the hybrid complexes in contrast to those of isolated molecules or sole NPs. Detailed investigations reveal that the AER is sensitive to the energy gap between the molecular excitation and plasmon modes. As anticipated, two separate absorption bands, corresponding to the isolated molecules and sole NPs, have been observed at the large energy gap. When the energy gap approaches to zero, the molecular excitation strongly couples with the plasmon mode to form the hybrid exciton band, which possesses the significantly enhanced absorption intensity, a red-shifted peak position, a surprisingly strongly asymmetric shape of absorption band, and the nonlinear Fano effect. Furthermore, the dependence of surface localized fields and the scattering response functions (SRFs) on the geometrical parameters of NPs, the NP-molecule separation distance, and the external-field polarizations has also

been depicted.

I. INTRODUCTION

It is known that the light can be guided and localized by metallic nanoparticles (NPs). As the light frequency is resonant with collective electron charge oscillations of NPs, the surface plasmon resonance (SPR) is formed[1], and this resonant excitation not only provides NPs with a brilliant optical property, but also offers an intensive surface localized field to enhance spectroscopic signals of molecules nearby[2–11]. To interpret the surface enhancement spectral signals, two well-accepted enhancement mechanisms have been proposed. One is the electromagnetic enhancement by the surface plasmon induced by an incident light, and the other is the chemical enhancement caused by the chemical interaction or a photo-induced charge transfer between the NPs and the molecules.

For the hybrid superstructures composed of NPs, molecules or semiconductors as building blocks in plasmonic devices and solar-cell design, however, it still meets a challenge for theoretical and computational methods to reveal the detailed enhancement information, because the optical properties of hybrid systems require a quantum mechanics (QM) description whereas the medium to large-size metal NPs are too large to be tackled by QM methods. Furthermore, the elementary excitations in molecules or semiconductors and metal NPs, an exciton and a plasmon, have very different properties, and the interaction between the plasmon and the exciton needs to be suitably tackled because it endows the hybrid superstructures the novel properties. To overcome those difficulties, many approaches have been proposed. For instance, it is assumed that the molecules are absorbed to very small metal clusters,[12,13] and then, the hybrid systems can be fully described by QM methods. However, small NPs may not support the bulk plasmon. The other ways include the effective Hamiltonian model[14,15], the semiclassical methods[9–11], and the mixed quantum/classical approaches where QM approaches and classical molecular mechanics or electrodynamics are jointed together. For example, Kerker *et. al.*[16] applied Mie theory to study electromagnetic field enhancements in surface enhancement Raman spectra, who considered a single molecule adsorbed on a metal sphere with the molecule treated as a classical point dipole. Govorov group[17,18] applied the coupled exciton-plasmon effective Hamiltonian model to study the carrier dynamics of semiconductor-metal nanostructures by solving the equation

of motion of the density matrix. In this model, the semiconductor was described by a two-state model or an exciton, the metal sphere was described by a series of semicontinuous states or the plasmon-induced localized electronic field, and the semiconductor-metal interaction was either described by the electromagnetic interaction or dipole-dipole interaction. Schatz's[19], Chen's[20], Neuhauser's[21] and Jensen's[22] groups applied the mixed quantum/classical approaches which combine TDDFT/time-dependent Hartree-Fock (TDHF) for adsorbates with the classical electrodynamics methods for the large metal NPs to investigate the surface-enhanced optical properties or the electron transport in nanodevices.

In this work, the optical properties of hybrid complexes assembled by the molecules and Ag NPs are investigated using the mixed quantum-classical approach, where the plasmon-induced localized field produced by the plasmon resonance of noble metal NPs, as usual, is obtained by the numerical solution of Maxwell's equations using the classical electrodynamics finite difference time domain (FDTD) technique, but the optical properties of the adsorbates are described by the real time (RT) TDDFT approaches.[23–35] In our RT-TDDFT approach[32], the molecular electronic evolution is described by the equation of motion of reduced one-electron density matrix without imposing the perturbation expansion. Therefore, the field-matter interaction, and the molecular internal Coulomb forces will be treated on equal footing. With this treatment, the molecular dynamic responses to two driving fields, the strong surface scattered field due to SPR and the weak incident electric field, can be well simultaneously described without the requirement of empirical parameters.

The major objective of this work is to describe the effect of the enhanced surface localized field generated by the SPR on the molecular optical absorption signals. We aim to make a quantitative description on the changes of spectral characters arisen by the interaction between the molecular excitons and metal NPs' plasmon modes. Meantime, we will depict the quantitative dependence of surface near-fields, the scattering response functions (SRFs), and the absorption enhancement ratio (AER) for each absorption band on the geometrical parameters of superstructures, the energy gap between the molecular excitation (ω_m) and plasmon mode (ω_p), the NP-molecule separation distance, and the external field polarization as well. The effect of plasmon-exciton coupling on the absorption spectra, the formation condition of hybrid exciton state, and its spectral behaviours will be further demonstrated.

The present investigation is useful for the development of nonlinear plasmonic devices, where a key aspect is the interaction of surface plasmon with optically active materials such as quantum dots, and it is also helpful for understanding the cavity quantum electrodynamics and designing approaches based on plasmonics to improve light absorption in photovoltaic devices and to yield new options for solar-cell design.

The rest of the paper is arranged as follows. In section II, we briefly describe the hybrid scheme for the molecular optical absorption spectroscopy. The details of RT-TDDFT coupled with FDTD method[36] through a SRF [19] are shown. In section III, we first investigate the dependence of surface scattered field on the NP size, the surface separation distance, and the orientation of NP pairs. The field enhancement factors are obtained by comparing the enhanced surface near field with the incident field. Then, the hybrid method is applied to calculate the surface-enhanced absorption of two dye molecules, spiropyran (SP) and merocyanine (MC), which have quite different absorption lineshapes and can be used as the model systems to explore how the AER is related to the energy gap of $|\omega_m - \omega_p|$, and what novel nonlinear property can be induced by the strong plasmon-exciton interaction. Finally, a concluding remark is given in section IV.

II. THEORETICAL METHODS

As an incident field irradiates on a hybrid system constructed by the NPs and an organic molecule, it interacts with the NPs and induces the oscillating multipoles on the latter creating an enhanced surface near field. The surface near field then interacts with the molecule and induces the molecular polarization, and the corresponding molecular absorption cross section can be obtained from the polarizability α

$$\sigma(\omega) \propto \frac{1}{3} \sum_{i=x,y,z} \omega \, \mathrm{Im}(\alpha_{ii}(\omega)). \tag{1}$$

Here the dynamic polarizability tensor is defined as $\alpha_{ij}(\omega) = \frac{\partial P_i(\omega)}{\partial E_j(\omega)}$, and $P_i(\omega)$ denotes the Fourier transform of the polarization $P_i(t) = Tr(\delta\rho(t)\mu_i)$, μ_i stands for the $i-$th component of the dipole moment. The field-induced one-electron density matrix (1DM) $\delta\rho(t) = \rho(t) - \rho(0)$ can be obtained by solving the equation of motion of the reduced one-electron density

matrix

$$i\hbar S\frac{d\rho(t)}{dt}S = F(t)\rho(t)S - S\rho(t)F(t). \quad (2)$$

Here S, ρ and F denote the overlap matrix, reduced one-electron density matrix and Fock matrix in atomic orbital basis, respectively. In the Fock matrix, one has to obviously include the field-matter interaction

$$F[\rho(t)] = F_0[\rho(t)] - \vec{E}_{total} \cdot \vec{\mu}, \quad (3)$$

where $\vec{E}_{total}$ denotes the surface near field interacting with the molecule, $\vec{E}_{total}(r,\omega) = \vec{E}_0(r,\omega) + \vec{E}_{sca}(r,\omega)$. $\vec{E}_0(r,\omega)$ and $\vec{E}_{sca}(r,\omega)$ denote the incident field and the surface scattered electric field produced by Ag NPs' plasmon, respectively. Assuming that the influence of the induced molecular multipoles to NPs' surface charges, and the carrier movement between the molecule and NPs are neglected, the surface near field generated by NPs can be obtained by solving the Maxwell's equations with use of FDTD method[36] subject to appropriate boundary conditions. By doing so, the plasmonic enhancement effect is considered on one hand, and the optical properties of the molecule close to Ag NPs is embodied on the other hand.

Eq.(2) can be solved in the time domain using the methods described in our previous paper[32]. The methods avoid the perturbation expansion of light-matter interaction, and the external laser field and the internal Coulomb forces of the atoms or molecules are thus treated on equal footing. In the concrete implementation, the Chebyshev expansion technique is used to propagate the reduced single-electron density matrix, and the modified midpoint and unitary transformation algorithm, originally developed to integrate the TDHF equations efficiently, are adopted to improve the computational efficiency. For the detailed description about the RT-TDDFT approaches, one may refer our previous papers[32,37]. The numerical implementation has been realized in the locally-modified Q-Chem software package[38]. In this work, all the RT-TDDFT calculations have been finished at the theoretical level of B3LYP/6-31G.

In order to quantitatively study the localized field near the surface of Ag NPs and connect the FDTD simulation to the RT-TDDFT calculations for the optical properties of nearby

molecule, we introduce a complex tensor SRF, $\lambda(r,\omega)$, by following Chen et.al[19],

$$\begin{aligned}\lambda_{i,j}(r,\omega) &= \frac{E_{i,total}(r,\omega)}{E_{j0}(r,\omega)} - \delta_{i,j} \\ &= \frac{\int dt e^{i\omega t} E_{i,total}(r,t)}{\int dt e^{i\omega t} E_{j0}(r,t)} - \delta_{i,j}. \end{aligned} \quad (4)$$

The SRF depends on both the propagation and the polarization directions of the incident light. A typical time-shifted Gaussian wave is chosen as the incident field in FDTD simulation in order to study a broad spectral range. Using the definition of $\lambda(r,\omega)$, the scattering electric field,$\vec{E}_{sca}(t)$, can be expressed as a two-dimensional Fourier transform of $\vec{E}_0(t)$ and $\lambda(\omega)$

$$\begin{aligned}E_{i,sca}(t) &= \frac{1}{2\pi}\int d\omega e^{-i\omega t} E_{i,sca}(\omega) \\ &= \frac{1}{2\pi}\int d\omega e^{-i\omega t} \sum_j \lambda_{i,j}(\omega) E_{j0}(\omega) \\ &= \frac{1}{2\pi}\int d\omega e^{-i\omega t} \sum_j \lambda_{i,j}(\omega) \int dt_1 e^{i\omega t_1} E_{j0}(t_1) \\ &= \frac{1}{2\pi}\sum_j \int\int d\omega dt_1 e^{i\omega(-t+t_1)} \lambda_{i,j}(\omega) E_{j0}(t_1). \end{aligned} \quad (5)$$

III. RESULTS AND DISCUSSION

A. Surface near fields and scattering response functions

The Maxwell's equations are solved using FDTD method within the JFDTD3D package[39]. In the calculations, the light propagation direction is fixed along the $+z$ axis in all FDTD simulations. A cubic simulation box with a side length of 40 nm is chosen and the grid size of 0.2 nm is adopted. Each grid cell is characterized by a uniform permittivity ε based on its distance to the center of the cubic box (the origin of the Cartesian frame), with $\epsilon(\omega) = \epsilon_\infty + \epsilon_D(\omega) + \sum_n \epsilon_{L,n}(\omega)$ inside the Ag NPs according to the Drude-Lorentz model and $\epsilon = 1$ in surrounding medium. Here ϵ_∞ is the relative permittivity, $\epsilon_D(\omega) = -\frac{\omega_p^2}{\omega(\omega+i\gamma)}$ is the relative permittivity resulted from Drude pole, ω_p is the bulk plasmon frequency, and γ is a width factor which includes electron-phonon and other intrinsic electron relaxation mechanisms. The last term, $\epsilon_{L,n}(\omega) = \frac{\Delta\epsilon_p \omega_p^2}{\omega_p^2 - \omega(\omega - i2\delta)}$, describes the relative permittivity arising from each Lorentz oscillator pole, where $\Delta\epsilon_p$ is the shift in relative permittivity for the

electron transition at plasmon mode ω_p and δ is the electron dephasing rate. For the chosen materials, all of the parameters has been determined from the experiment[40]. The incident light pulse with the functional form, $E_0(t) = e^{-(t-t_0)^2/\sigma^2} sin(\omega_0 t)$, was injected from the plane at $z = -16$, where $t_0 = 10.0$ fs, $\sigma = 0.7$ fs, and $\omega_0 = 600.0$ nm. These pulse parameters can make the incident laser pulse fully cover the visible spectrum from 300 to 800 nm. The total simulation time is 100 fs and the time step size is 3.66×10^{-4}fs.

Figs. 1(a) and 2(a) show the contours of surface near field observed in a xy plane when the incident laser pulse is assumed to have a polarization direction along $+x$ and $+y$ axis, respectively. The electric field has been normalized with respect to the incident field. The 'hot spots' very clearly shows that a strong near field appears close to the surface, and that the light scattering from this small Ag metal NP embedded in a homogeneous medium is nearly symmetric in the forward and backward directions. A clear comparison between the simulated surface near fields and the incident electric fields is shown in the supporting information. It is apparent that the surface near fields have been obviously enhanced compared with the incident electric field. However, the enhancement factor of the near field is very much dependent on the NP size, the surface separation distance and the incident field polarization as well.

The properties of SRF tensors are shown in Figs.1 and 2, where only the diagonal components $\lambda_{\sigma,\sigma}$ are displayed because the off-diagonal components are negligibly small. As the propagation direction of the incident light is along the z axis, the diagonal terms of tensor would only involve λ_{xx} and λ_{yy}. Therefore, two separated FDTD simulations were carried out by assuming the incident field is polarized along the x and y directions, respectively. The variations of real and imaginary parts of λ_{xx} and λ_{yy} vs the NP sphere radium R and the separation distance L are displayed in Figs. 1 and 2 (b) and (c).

At first, we check the variation of λ versus the observation point, which is always set along the x axis and is marked as 'O' in Figs.1 and 2. It is expected that the amplitudes of real and imaginary parts of λ_{xx} and λ_{yy} should decrease as L increases. For NP with $R = 5$ nm, there is a featured peak centered at about 3.5 eV in the $Im(\lambda)$, which is ascribed to the plasmon mode. $Im(\lambda)$ is pertinent to the light absorption of NPs. At all the given observation points along the x axis, the lineshapes of λ_{xx} and λ_{yy} look like. But λ_{xx} is always

significantly larger than λ_{yy}. This is because in both cases, the fields are recorded at the same observation point along the x axis. Therefore, it is comprehensible that the strength of λ_{yy} is smaller than λ_{xx}.

The effect of NP size on SRFs is significant. As R increases from 5 to 12 nm, the amplitudes of SRFs decrease and the plasmon band widths increase. In fact, as the size of Ag NP gets increased, the intensity of the total electric field can be strengthened and its duration gets shortened as shown in the supporting information. These two contradictory factors cause the diagonal components of tensor SRFs weakened as R increases. Besides, we observe that the plasmon mode gets red-shifted with increasing R. There should exist convergence behavior of these size-dependent features in a "large particle" limit. For large NPs, the dipole approximation is no longer valid. The larger the NP becomes, the more important the higher-order modes become as the light can no longer polarize the NPs homogeneously. These higher-order modes typically locate at lower energies and thus cause the plasmon band gets red-shifted with the increasing of particle size[41–43].

While the size effect is very apparent, the particle arrangement effect seems to be even more pronounced in the plasmon resonance of Ag NPs. In Fig. 3(a)and (b), we set two Ag NPs in different ways. Two silver spheres have the same radii of $R = 5$ nm and the distance of the two sphere centers is 12 nm. When the external field is polarized along the dimer axis, the 'hot spots' between two NPs is formed, the induced localized field in the gap of two NPs is much stronger than the incident field. Fig. 3(c) shows the real and imaginary parts of λ_{xx} at the given observation point. Obviously, the constructive interference of two dipoles induced in each particle makes the plasmon on the surface more active, and the interaction also redshifts the plasmon mode. For dimer along y axis, the induced dipole in each NP is nearly parallel so that the field intensity at the point 'O' in Fig. 3(b) is almost the same with that generated by the single NP. However, the interaction between two NPs in this case blueshifts the plasmon mode a little comparing to that produced by the single NP.

B. Surface enhanced absorption of spiropyran and merocyanine

Then we apply the hybrid RT-TDDFT/FDTD scheme to study the optical properties of NP-molecule systems. Two dye molecules, SP and MC, are used as a test set to investigate the surface enhancement of the molecular light absorption. As shown in Fig.4, the MC and SP molecules have quite different optical absorption properties, which would allow us to check the relevance of the absorption enhancement behavior with the energy gap between the molecular excitation and and plasmon excitation.

In order to get the absorption spectra of a board energy range, we apply a weak short-duration laser pulse with Gaussian function envelope, $E_0(t) = (E/\sqrt{\pi}\tau)e^{-(t-\bar{t})^2/\tau^2}$, where $E = 1.0 \times 10^{-4}$ a.u., $\bar{t} = 0.0$, and $\tau = 1.0$ a.u.. Since the off-diagonal terms of $\lambda(r,\omega)$ are nearly negligible compared with the diagonal terms, only λ_{xx} and λ_{yy} are involved in the spectral calculations. To compare the theoretical spectra directly with the experimental spectra, two separated RT-TDDFT simulations have been carried out by assuming the incident electric field pulse applied along $x-$ and $y-$axis, respectively, and then the average absorption cross sections $\frac{\sigma_{xx}+\sigma_{yy}}{2}$ have been calculated.

Firstly, the electronic excitations of isolated MC and SP molecules are examined by applying RT-TDDFT approach. Their geometries are optimized at B3LYP/6-31G level and displayed in the inset of Fig. 4(a) and (c). The SP molecule has a non-planar geometry while the MC molecule is planar. For the isolated MC molecule, theoretical results reveal that the lowest-energy absorption peak at 2.5 eV has the maximum absorption intensity. Another sharp peak locates at about 3.3 eV with a nearby shoulder at 3.5 eV. In the high-energy range, two main absorption bands at 4.2 and 5.1 eV are observed. The calculated absorption profiles agree well with the experimental measurement on the molecule films[44]. The excitations at 2.5 eV and 3.3 eV mainly come from the electronic transitions along $x-$axis, and the excitation at 3.5 eV mainly comes from those along y-axis. For the isolated SP molecule, a major absorption peak at 3.5 eV was theoretically predicted (see Fig.4(c)), which mainly comes from the electronic transitions along $x-$axis and nearly resonates with the plasmon excitation of Ag sphere with $R = 5$ nm.

Then the MC molecule is set along the $x-$axis near a silver sphere of $R = 5$ nm with

varying separation distance L (for the explicit orientation of the molecule, see Fig. 4(a)). The absorption cross sections σ_{xx} and $\frac{\sigma_{xx}+\sigma_{yy}}{2}$ of NP-MC system are calculated. The absorption cross sections of isolated MC molecule at the same condition are also displayed in Figs. 5(a) and (b) for the comparison. Obviously, the enhanced surface electric field amplifies the molecular absorption in the whole energy range of $0-7$ eV, and strongly alters the absorption profiles of NP-bound systems in contrast to the isolated NPs or molecules. The plasmon enhancement effect decreases with the increasing of L. As L increases, the intensity of scattered electric field becomes weak, which can be directly associated with decrease of the absorption cross section. The AER for the absorption band near the plasmon mode gets profoundly amplified compared with those away from the plasmon mode. This is evidenced by the values in Figs. 5(a) and (b). Notably, the absorption cross sections around ω_p decrease very quickly as L increases, leading to the peak at 3.5 eV evolves to a shoulder of that at 3.3 eV in NP-bound MC system.

To have a clearer demonstration on the AER of each absorption band, we plot the variations of AERs of three low-lying excited states vs the separation distance L and NP radius R in Fig. 6. The plot clearly demonstrates that the smaller the separation distance L and the energy difference of $|\omega_m - \omega_p|$ are, the larger the AER becomes. Due to the different AER for each absorption band, the spectral lineshapes of NP-bound MC system is significantly different from those of isolated MC molecule or sole NPs. For σ_{xx} of NP-MC system at $L = 1$ nm, the strongest absorption enhancement appears at the band of 3.3 eV, which has been magnified by 32 times and becomes the dominant one. Besides, a new sharp peak appears at about 3.5 eV, which can be ascribed to the plasmon mode. By comparing Fig. 5(b) with Fig. 5(a), it is clear that the major difference lies in the bands near the plasmon mode. Due to the resonance between the molecular excitation at 3.5 eV and the plasmon excitation of NP with $R = 5$ nm, the strongest enhancement in $\frac{\sigma_{xx}+\sigma_{yy}}{2}$ of NP-MC system occurs at the peak 3.5 eV, which is enhanced at least 56 times at $L = 1$ nm shown in Fig. 6(a). On the red side of the plasmon mode, the lowest-energy peak at 2.5 eV is amplified by about 8 times. There is a small enhancement on the blue side of the plasmon mode where the enhancement ratio is just about 1.5. The strong plasmon-exciton interaction also causes the absorption peaks around the plasmon mode get shifted weakly. It is observed that the absorption peaks

at 3.5 and 3.3 eV get red-shift and blue-shift about 0.01 eV, respectively, in contrast with that of isolated MC molecule.

The resonance enhancement can be found more clearly for the NP-SP system. For the isolated SP molecule, there is a strong sharp absorption peak at 3.5 eV, which nearly has the same excitation frequency with that of the plasmon excitation of Ag NP with $R = 5$ nm. Due to the resonance between the molecular excitation and the plasmon excitation of Ag sphere with $R = 5$ nm, two-types of excitations are strongly coupled, leading to an unusual absorption enhancement for the band at 3.5 eV (see Fig. 7). In this case, one can not distinguish the molecular excitation band from the plasmon mode, and a hybrid exciton band is formed. The abnormal behaviours of this band can also be reflected by the significant red-shift of the peak position and the appearance of strongly asymmetric shape of absorption band. The absorption peak at 3.5 eV red-shifts about 0.04 eV. And there even exists a slightly negative absorption cross section appeared at the blue side of the plasmon band. These phenomena originate from the coherent NP-molecule interaction and can be viewed as a nonlinear Fano effect, which is quite different from the usual linear Fano resonance[17,45]. It is known that this nonlinear Fano effect strongly depends on the incident field intensity. We expect that the small negative peak in absorption cross section will gradually disappear with the decreasing incident electric-field intensity. In our model, the molecule interacts with two fields, one is the intensive scattered field and the other is weak external incident field. When the scattered field behaves like a resonant driving field strong enough to produce population saturation, the stimulated emission phenomena may appear when another weak incident field was applied on the molecule[46].

The NP size also has a significant effect on the optical properties of NP-molecule systems. Keeping $L = 1$ nm unchanged, we calculate the absorption spectra of NP-MC and NP-SP systems with the different NP size (R varies from 5, 10 to 12 nm). As shown in Figs. 5(c) and 7, as R increases, the intensity of the peak at 3.3 eV significantly increases and that at 3.5 eV decreases for both hybrid systems, which further support the conclusion that the AER is very sensitive to the energy difference of $|\omega_m - \omega_p|$. From the SRFs, we have known that the plasmon band would undergo apparent changes as the size of NP increases. One primary plasmon mode at 3.5 eV in the NP with $R = 5$ nm becomes two plasmon bands

in NPs with $R = 10$ and 12 nm. The wider and weaker plasmon bands in the larger NPs weaken the coupling between the plasmon modes and molecular exciton at 3.5 eV so that the AER of the band close to 3.5 eV are largely decreased. However, as the plasmon band red-shifts with the increasing of R, the coupling between the plasmon excitation and the molecular excitation at 3.3 eV becomes stronger, and a normal increasing absorption cross section for the peak at 3.3 eV is observed.

At the microscopic level, the molecular absorption spectral differential cross section can be explicitly written as $\sigma(\omega) = \frac{4\pi^2\omega}{3c} Im \sum_F \sum_x \frac{(\mu_{IF}^x)^2}{\omega_{FI}-\omega-i\gamma_F}$. $|I\rangle$ and $|F\rangle$ denote the initial and final states and ω denotes the incident photon frequencies. $\vec{\mu}$ is the molecular dipole operator. In the presence of NPs, the electric-field enhancement inside a molecule due to the presence of NPs will change the molecular transition dipole moments to $\hat{\mathcal{P}}\vec{\mu}_{FI}$. Here $\hat{\mathcal{P}}$ denotes the electric-field enhancement matrix. Meantimes, the plasmon mode of NPs and the induced-polarization of molecule will also interact to affect the absorption lineshape. Therefore, the interaction between NPs and molecules will not only change the spectral intensities but also change the spectral positions. We thus observed that the shifted value of the peak position also depends on the superstrucrure's geometric parameters, the energy gap of $|\omega_p - \omega_m|$, and the intensity of the incident electric field.

The resonance enhancement phenomena have been applied in the development of the plasmonics-based nanodevices and solar cells. For example, to improve the dye-sensitized solar cells (DSSC) performance associated with plasmon excitation, people developed the multilayer fabrication strategies for plasmonic DSSCs by anchoring the dye molecules on the surface of TiO2-coated plasmonic (silver or gold) particles,[47] where a key strategy is to reach a perfect match between the absorption maxima of the dye and the plasmon wavelength of SiO2-coated Au nanoparticles when both of them are integrated into mesoporous TiO2. Chen et.al. has performed a computational study on plasmon-enhanced light absorption in a multicomponent DSSC,[48] and clearly demonstrated that the light absorption can be significantly enhanced at the plasmon wavelength of 462 nm for most positions of the N3 dye on the nanoparticle surface.

Finally, we study the absorption enhancement effect of MC molecule subject to two identical Ag NPs (Fig. 8). Two NPs with the same radii (R=5 nm) are arrayed along x

axis, and the distance between two sphere centers is fixed to be 12 nm. The MC molecule is set in the gap of two Ag NPs and is 1 nm away from each silver surface. As Fig. 3(a) shows, the interaction between NPs builds a rather strong localized filed between them, which significantly enhances the absorption of the MC molecule throughout the whole energy range. An unusual enhancement appears on the band at 3.3 eV. This on-resonance enhancement ratio reaches to a maximum value of 1260. Although the absorption at other energy range is also enhanced, the corresponding AER is significantly smaller than that at 3.3 eV. As a result, the absorption band at 3.3 eV becomes the dominant one, and other peaks except the one at 2.5 eV are almost invisible.

IV. CONCLUDING REMARKS

The hybrid scheme which combines the RT-TDDFT approach for the dynamic polarizibilities of adsorbates with the FDTD method for the solution of Maxwell's equations has been demonstrated to be well suitable for systematically investigating the Plasmon-enhanced light absorption. The FDTD results have shown that the surface localized field generated by SPR of Ag NPs strongly depends on the NP's geometrical parameters, the surface separation distance, incident-field polarization, and it can be strengthened by increasing the NP sizes or forming a crevice between NPs. However, the amplitudes of SRFs don't increase as the NP sphere radii increase. The plasmon band gets red-shifted with increasing NP size or through formation of a crevice between NPs.

For the molecule near the Ag NPs, its absorption enhancement caused by the surface localized field heavily depends on the energy gap between the molecular excitation and plasmon mode. As the energy gap is sufficient large, the coupling between the plasmon mode and molecular transition dipole moment can be neglected so that two separate absorption bands, one from the isolated molecule excitation and the other from the plasmon excitation, have been observed as anticipated. As the energy gap approaches to zero, the molecular excitation strongly couples with the plasmon excitation to form the hybrid exciton band, which possesses the significantly amplified absorption intensity and shifted peak position compared with the isolated molecular excitation. It is thus concluded that the interaction

between NPs and molecules not only enhances the spectral intensities but also modifies the spectral profiles.

When the incident field is strong enough, the joint effect of the incident field and the strong scattering field generated by SPR of NPs can induce some novel nonlinear phenomena, such as the population saturation on the molecular excited state, the red-shift spectral position and a surprising strongly asymmetric shape of absorption band in the range of Ag plasmon band. Furthermore, even slightly negative absorption peaks have been observed, which have been explained by a possible nonlinear Fano effect.

The present study demonstrates that the mixed TDDFT/FDTD methodology could provide a useful computational tool to describe the plasmon-enhancement light absorption behaviours. This work is useful for the development of nonlinear plasmonic devices, where a key aspect is the interaction of surface plasmon with optically active materials such as quantum dots, and it is also helpful for understanding the cavity quantum electrodynamics and designing approaches based on plasmonics to improve absorption in photovoltaic devices and to yield new options for solar-cell design.

AUTHOR INFORMATION

Corresponding Author

*E-mail: liangwz@xmu.edu.cn

Notes

The authors declare no competing financial interest.

ACKNOWLEDGMENTS

The Project was supported by the National Natural Science Foundation of China (Grant No: 21103001, No: 21373163 and No. 21290193) and Research Foundation for the Doctoral Program of Higher Education of China (20113401120004). JS thanks the financial support from the state key laboratory of physical chemistry of solid surfaces, XMU.

Supporting Information Available:

The time-dependent surface localized fields generated by Ag NPs by FDTD scheme, the vertical excitation energies and transition dipole moments of MC and SP molecules calculated by the conventional TDDFT approach within Q-Chem package at TD-B3LYP/6-31G theoretical level.

REFERENCES

[1] M. A. El-Sayed, Some Interesting Properties of Metals Confined in Time and Nanometer Space of Different Shapes. *Acc. Chem. Res.*, 2001, **34**, 257-264.

[2] A. J. Haes, S. L. Zou, G. C. Schatz, R. P. Van Duyne, Nanoscale Optical Biosensor: Short Range Distance Dependence of the Localized Surface Plasmon Resonance of Noble Metal Nanoparticles. *J. Phys. Chem. B*, 2004, **108**, 6961-6968.

[3] M. Danckwerts, L. Novotny, Optical Frequency Mixing at Coupled Gold Nanoparticles. *Phys. Rev. Lett.*, 2007, **98**, 026104.

[4] N. T. Fofang, T.-H. Park, O. Neumann, N. A. Mirin, P. Nordlander, N. J. Halas, Plexcitonic Nanoparticles: Plasmon-Exciton Coupling in Nanoshell-J-Aggregate Complexes. *Nano Lett.*, 2008, **8**, 3481-3487.

[5] J. B. Lassiter, H. Sobhani, J. A. Fan, J. Kundu, F. Capasso, P. Nordlander, N. J. Halas, Fano Resonances in Plasmonic Nanoclusters: Geometrical and Chemical Tunability. *Nano Lett.*, 2010, **10**, 3184-3189.

[6] M. Pelton, J. Aizpurua, G. Bryant, Metal-Nanoparticle Plasmonics. *Laser & Photon.*, 2008, **2**, 136-159.

[7] T. Shegai, Z. Li, T. Dadosh, Z. Zhang, H. Xu, and G. Haran, Managing Light Polarization via Plasmon-Molecule interactions within an Asymmetric Metal Nanoparticle Trimer. *Pro. Nat. Aca. Sci.*, 2008, **105**, 16448-16453.

[8] H. Atwater, The Promise of Plasmonics. *Sci Am*, 2007, **296**, 56-63.

[9] Y. S. Kim, P. T. Leung, T. F. George, Classical Decay Rates for Molecules in the Presence of a Spherical Surface: A Complete Treatment. *Surf. Sci*, 1988, **195**, 1-14.

[10] H. Mertens, A. F. Koenderink, A. Polman, Plasmon-Enhanced Luminescence Near Noble-Metal Nanospheres: Comparison of Exact Theory and an Improved Gersten and Nitzan Model. *Phys. Rev. B*, 2007, **76**, 115123.

[11] D. V. Guzatov, S. V. Vaschenko, V. V. Stankevich, A. Y. Lunevich, Y. F. Glukhov, S. V. Gaponenko, Plasmonic Enhancement of Molecular Fluorescence Near Silver Nanoparticles: Theory, Modeling, and Experiment. *J. Phys. Chem. C*, 2012, **116**, 10723-10733.

[12] L. Zhao, L. Jensen, G. C. Schatz, Pyridine-Ag_{20} Cluster: A Model System for studying Surface-Enhanced Raman Scattering. *J. Am. Chem. Soc.*, 2006, **128**, 2911-2919.

[13] J. F. Arenas, J. Soto, I. L. Tocon, D. J. Fernandez, J. C. Otero, J. I. Marcos. *J. Chem. Phys.* 2002, **116**, 7207.

[14] B. N. J. Persson, On the Theory of Surface-enhanced Raman Scattering, *Chem. Phys. Lett.* 1981, **82**, 561.

[15] Y. Zhao, W. Z. Liang, Theoretical Investigation of Resonance Raman Scattering of Dye Molecules Absorbed on Semiconductor Surfaces, *J. Chem. Phys.* 2011, **135**, 044108.

[16] M. Kerker, D.-S. Wang, H. Chew, Surface Enhanced Raman Scattering (SERS) by Molecules Adsorbed at Spherical Particles: Errata. *Appl. Optics.*, 1980, **19**, 4159-4174.

[17] W. Zhang, A. O. Govorov, G. W. Bryant, Semiconductor-Metal Nanoparticle Molecules: Hybrid Excitons and the Nonlinear Fano Effect. *Phys. Rev. Lett.*, 2006, **97**, 146804.

[18] (a) J.-Y. Yan, W. Zhang, S. Duan, X.-G. Zhao, A. O. Govorov, Optical Properties of Coupled Metal-Semiconductor and Metal-Molecule Nanocrystal Complexes: Role of Multipole Effects. *Phys. Rev. B*, 2008, **77**, 165301. (b) A. O. Govorov, Z. Fan, P. Hernandez, J. M. Slocik, R. R. Naik, Theory of Circular Dichroism of Nanomaterials Comprising Chiral Molecules and Nanocrystals: Plasmon Enhancement, Dipole Interactions, and Dielectric Effects. *Nano Lett.*, 2010, **10**, 1374-1382

[19] H. Chen, J. M. McMahon, M. A. Ratner, G. C. Schatz, Classical Electrodynamics Coupled to Quantum Mechanics for Calculation of Molecular Optical Properties: a RT-TDDFT/FDTD Approach. *J. Phys. Chem. C.*, 2010, **114**, 14384-14392.

[20] L. Y. Meng, Z. Y. Yin, C. Y. Yam, S. K. Koo, Q. Chen, N. Wong, G. H. Chen, Frequency-Domain Multiscale Quantum Mechanics/Electromagnetics Simulation Method. *J. Chem. Phys.*, 2013, **139**, 244111.

[21] (a) Y. Gao, D. Neuhauser, Dynamical quantum-electrodynamics embedding: Combinning time-dependent density functional theory and the near-field method. *J.Chem.Phys.*, 2012, **137**, 074113. (b) D. Neuhauser, K. Lopata, Molecular nanopolaritonics: Cross manipulation of near-field plasmons and molecules. I. Theory and application to junction control. *J. Chem. Phys.*, 2007, **127**, 154715.

[22] (a) S. M. Morton and L. Jensen, A Discrete Interaction Model/Quantum Mechanical Method to Describe the Interaction of Metal Nanoparticles and Molecular Absorption, *J. Chem. Phys.*, 2011, **135**, 134103. (b) J. L. Payton, S. M. Morton and L. Jensen, A Hybrid Atomistic Electrodynamics-Quantum Mechanical Approach for Simulating Surface-enhanced Raman Scattering, *Acc. Chem. Res.*, 2014, **47**, 88-99.

[23] K. Yabana, G. F. Bertsch, Time-Dependent Local-Density Approximation in real time. *Phys. Rev. B.*, 1996, **54**, 4484-4487.

[24] (a) C. Y. Yam, S. Yokojima, G. H. Chen, Linear-Scaling Time-Dependent Density-Functional Theory. *Phys. Rev. B*, 2003, **68**, 153105. (b) C. Y. Yam, S. Yokojima, G. H. Chen, Localized-Density-Matrix Implementation of Time-Dependent Density-Functional Theory. *J. Chem. Phys.*, 2003, **119**, 8794.

[25] A. Castro, M. A. L. Marques, A. Rubio, Propagators for the Time-Dependent Kohn-Sham equations. *J. Chem. Phys.*, 2004, **121**, 3425.

[26] K. Yabana, T. Nakatsukasa, J.-I. Iwata, G. F. Bertsch, Real-Time, Real-Space Implementation of the Linear Response Time-Dependent Density-Functional Theory. *Phys. Status Solidi B*, 2006, **243**, 1121.

[27] C. L. Cheng, J. S. Evans, T. V. Voorhis, Simulating Molecular Conductance Using Real-Time Density Functional Theory. *Phys. Rev. B*, 2006, **74**, 155112.

[28] M. Pi, F. Ancilotto, E. Lipparini, R. Mayol, Magneto-Optics of Three-Dimensional Quantum Dots: A Real Time, Time-Dependent Local Spin-Density Approach. *Physica E*, 2004, **24**, 297-307.

[29] M. A. L. Marques, A. Castro, G. F. Bertsch, A. Rubio, Octopus: A First-Principles Tool for Excited Electron-Ion Dynamics. *Comput. Phys. Commun.*, 2003, **151**, 60-78.

[30] (a)R. Baer, Accurate and Efficient Evolution of Nonlinear Schrödinger Equations. *Phys. Rev. A*, 2000, **62**, 063810. (b) R. Baer, R. Gould, A Method for ab Initio Nonlinear Electron-Densty Evolution. *J. Chem. Phys.*, 2001,**114**, 3385. (c) R. Baer, Y. Kurzweil, L. S. Cederbaum, Time-Dependent Density Functional Theory for Nonadiabatic Processes. *Israel J. Chem.*, 2005,**45**, 161-170.

[31] A. Tsolakidis, D. Sánchez-Portal, R. M. Martin, Calculation of the Optical Response of Atomic Clusters Using Time-Dependent Density Functional Theory and Local Orbitals. *Phys. Rev. B*, 2002, **66**, 235416.

[32] J. Sun, J. Song, Y. Zhao, W. Z. Liang, Real-Time Propagation of the Reduced One-Electron Density Matrix in Atom-Centered Gaussian Orbitals: Application to Absorption Spectra of Silicon Clusters. *J. Chem. Phys.*, 2007, **127**, 234107.

[33] J. Sun, J. Liu, W.Z. Liang, Y. Zhao, Real-Time Propagation of the Reduced One-Electron Density Matrix in Atom-Centered Orbitals: Application to Multielectron Dynamics of Carbon Clusters C_n in the Strong Laser Pulses. *J. Phys. Chem.*, 2008, **112**, 10442-10447.

[34] F. Wang, C. Y. Yam, G. Chen, K. Fan, Density Matrix Based Time-Dependent Density Functional Theory and the Solution of Its Linear Response in Real Time Domain. *J. Chem. Phys.*, 2007, **126**, 134104.

[35] (a) X. S. Li, J. C. Tully, H. B. Schlegel, M. J. Frisch, Ab Initiao Ehrenfest Dynamics. *J. Chem. Phys.*, 2005, **123**, 084106. (b) X. S. Li, S. M. Smith, A. N. Markevitch, D. A. Romanov, R. J. Levis, H. B. Schlegel, A Time-Dependent Hartree-Fock Approach for Studying the Electronic Optical Response of Molecules in Intense Fields. *Phys. Chem. Chem. Phys.*, 2005, **7**, 233-239. (c) C. M. Isborn, X. S. Li, J. C. Tully, Time-Dependent Density Functional Theory Ehrefest Dynamics: Collisions Between Atomic Oxygen and Graphite Clusters. *J. Chem. Phys.*, 2007, **126**, 134307.(d) H. B. Schlegel, S. M. Smith, X. S. Li, Electronic Optical Response of Molecules in Intense Fields: Comparison of TD-HF, TD-CIS, and TD-CIS(D) Approaches. *J. Chem. Phys.*, 2007, **126**, 244110. (e) S. M. Smith, X. S. Li, A. Markevitch, D. Romanov, R. J. Levis, H. B. Schlegel, Numerical Simulation of Nonadiabatic Electron Excitation in the Strong-Field Regime.

3. Polyacene Neutrals and Cations. *J. Phys. Chem. A*, 2007, **111**, 6920-6932.

[36] E. K. Miller, Time-Domain Modeling in Electromagetics. *J.Electromagn. Waves Appl.*, 1994, **8**, 1125.

[37] J. Liu, Z. Y. Guo, J. Sun, W. Z. Liang, Theoretical Studies on Electronic Spectroscopy and Dynamics with the Real-Time Time-Dependent Density Functional Theory. *Frontier of Chemistry.*, 2010, **5**, 11.

[38] Y. H. Shao, L. F. Molnar, Y. S. Jung, J. Kussmann, C. Ochsenfeld, S. T. Brown, A. T. B. Gilbert, L. V. Slipchenko, S. V. Levchenko, D. P. O¡¯Neill, R. A. DiStasio, R. C. Lochan, T. Wang, G. J. O. Beran, N. A. Besley, J. M. Herbert, C. Y. Lin, T. Van Voorhis, S. H. Chien, A. Sodt, R. P. Steele, V. A. Rassolov, P. E. Maslen, P. P. Korambath, R. D. Adamson, B. Austin, J. Baker, E. F. C. Byrd, H. Dachsel, R. J. Doerksen, A. Dreuw, B. D. Dunietz, A. D. Dutoi, T. R. Furlani, S. R. Gwaltney, A. Heyden, S. Hirata, C. P. Hsu, G. Kedziora, R. Z. Khalliulin, P. Klunzinger, A. M. Lee, M. S. Lee, W. Liang, I. Lotan, N. Nair, B. Peters, E. I. Proynov, P. A. Pieniazek, Y. M. Rhee, J. Ritchie, E. Rosta, C. D. Sherrill, A. C. Simmonett, J. E. Subotnik, H. L. Woodcock, W. Zhang, A. T. Bell, A. K. Chakraborty, D. M. Chipman, F. J. Keil, A. Warshel, W. J. Hehre, H. F. Schaefer, J. Kong, A. I. Krylov, P. M. W. Gill, M. Head-Gordon, Advances in methods and algorithms in a modern quantum chemistry program package. *Phys. Chem. CHem. Phys.*, 2006, **8**, 3172-3191.

[39] J. M. McMahon, Y. Wang, L. J. Sherry, R. P. Van Duyne, L. D. Marks, S. K. Gray, G. C. Schatz, Correlating the Structure, Optical Spectra, and Electrodynamics of Single Silver Nanocubes. *J. Phys. Chem. C.* 2009, **113**, 2731-2735.

[40] P. B. Johnson, R. W. Christy, Optical Constants of the Noble Metals. *Phys. Rev. B*, 1972, **6**, 4370.

[41] *Optical Properties of Metal Clusters*, ed. U. Kreibig and M. Vollmer, Springer-Verlag: New York press, 1995.

[42] S. Link, M. A. EI-Sayed, Shape and Size Dependence of Radiative, non-Radiative and Photothermal Properties of Gold Nanocrystals. *Int. Rev. Phys. Chem.*, 2000, **19**, 409-453.

[43] K. M. Mayer, J. H. Hafner, Localized Surface Plasmon Resonance Sensors. *Chem.Rev.*, 2011, **111**, 3828-3857.

[44] J. A. Hutchison, T. Schwartz, C. Genet, E. Devaux, T. W. Ebbesen, Modifying Chemical Landscapes by Coupling to Vacuum Fields. *Angew.Chem.Int.Ed.*, 2012, **51** 1592-1596.

[45] M. Kroner, A. O. Govorov, S. Remi, B. Biedermann, S. Seidl, A. Badolato, P. M. Petroff, W. Zhang, R. Barbour, B. D. Gerardot, R. J. Warburton, K. Karrai, The Nonliear Fano Effect. *Nature*, 2008, **451**, 311-314.

[46] F. Y. Wu, S. Ezekiel, M. Ducloy, B. R. Mollow, Observation of Amplification in a Strongly Driven Two-Level Atomic System at Optical Frequencies. *Phys. Rev. Lett.* , 1977, **38**, 1077-1080.

[47] (a) C. Hagglund, M. Zach, B. Kasemo, Enhanced charge carrier generation in dye sensitized solar cells by nanoparticle plasmons. *Appl. Phys. Lett.* 2008, **92**, 013113-3. (b) S. D. Standridge, G. C. Schatz, J. T. Hupp, Distance Dependence of Plasmon-Enhanced Photocurrent in Dye-Sensitized Solar Cells. *J. Am. Chem. Soc.* 2009, **131**, 8407-8409. (c) M. D. Brown, T. Suteewong, R. S. S. Kumar, V. D'Innocenzo, A. Petrozza, M. M. Lee, U. Wiesner, H. J. Snaith, Plasmonic Dye-Sensitized Solar Cells Using Core-Shell Metal-Insulator Nanoparticles, *Nano Lett.* 2010, **11**, 438-445.

[48] H. Chen, M. G. Blaber , S. D. Standridge , E. J. DeMarco , J. T. Hupp , M. A. Ratner , and G. C. Schatz, Computational Modeling of Plasmon-Enhanced Light Absorption in a Multicomponent Dye Sensitized Solar Cell. *J. Phys. Chem. C*, 2012, **116**, 10215-10221.

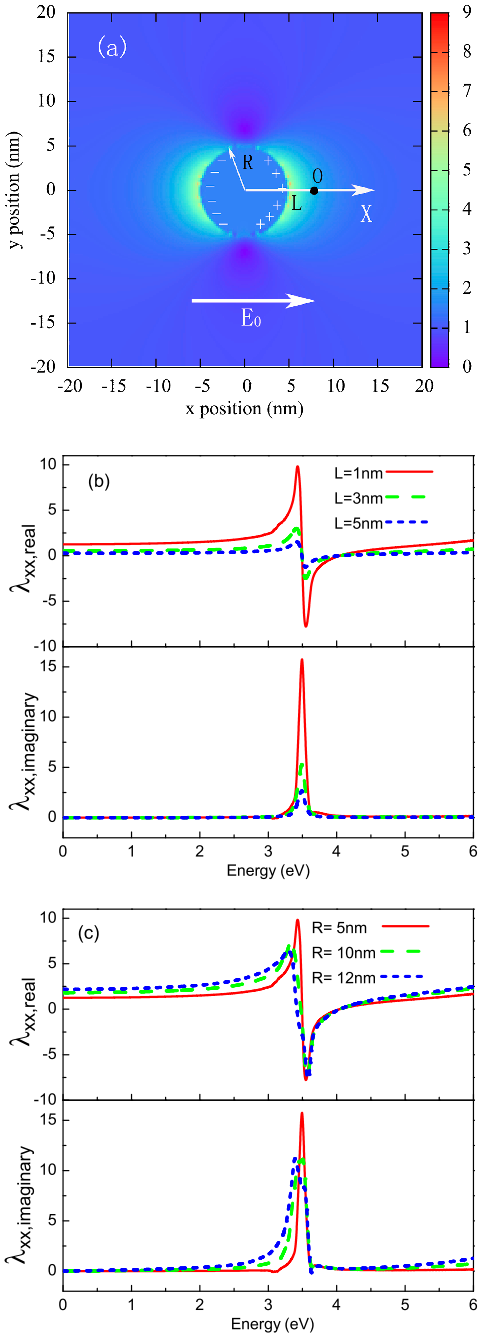

FIG. 1: (a) The contour of surface localized field generated by a Ag NP sphere with $R = 5$ nm. The arrow denotes the field polarization direction. The magnitude of the field intensity E is indicated by the colour scale. The observation point 'O' is set in the x-axis and is away from the NP surface with a distance of L. (b) The real and imaginary parts of λ_{xx} at $R = 5$ nm, and $L = 1$, 3 and 5 nm, respectively. (c)The real and imaginary parts of λ_{xx} at $R = 5$, 10 and 12 nm, and $L = 1$ nm.

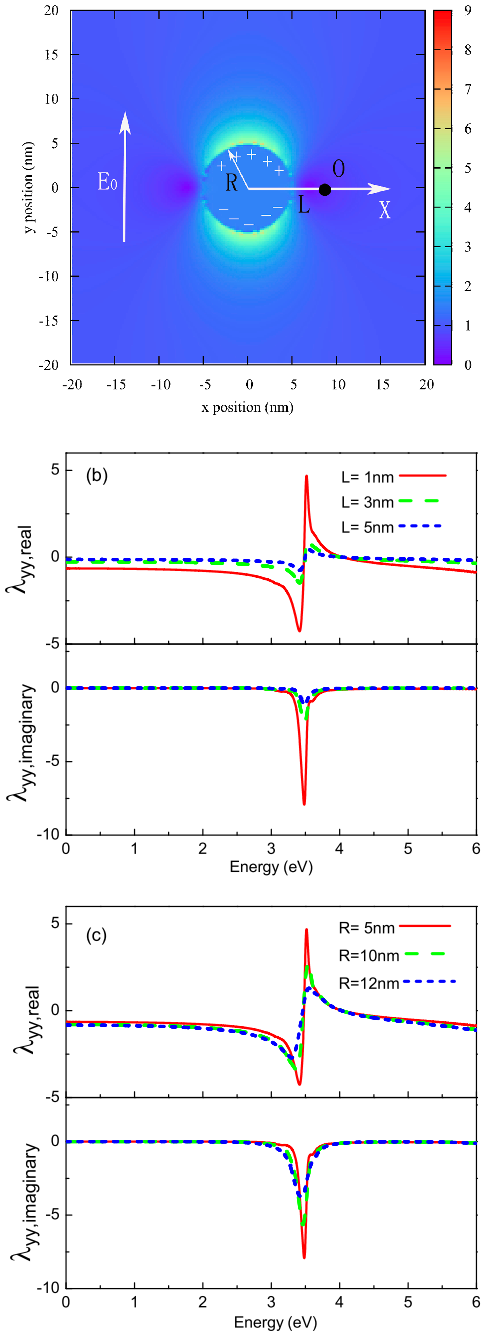

FIG. 2: The same condition with that in Fig.1 is set, except the field polarization direction (along y-axis).

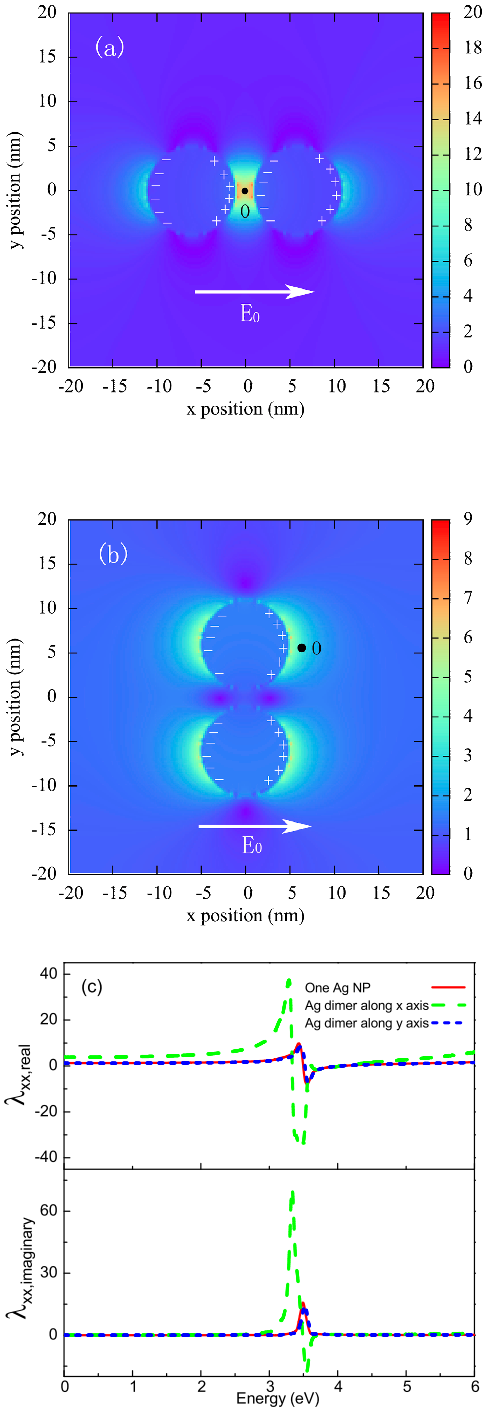

FIG. 3: (a) and (b) The contours of surface localized fields produced by two NP dimers with $R = 5$ nm. (c) The real and imaginary parts of λ_{xx} at the observation point 'O'.

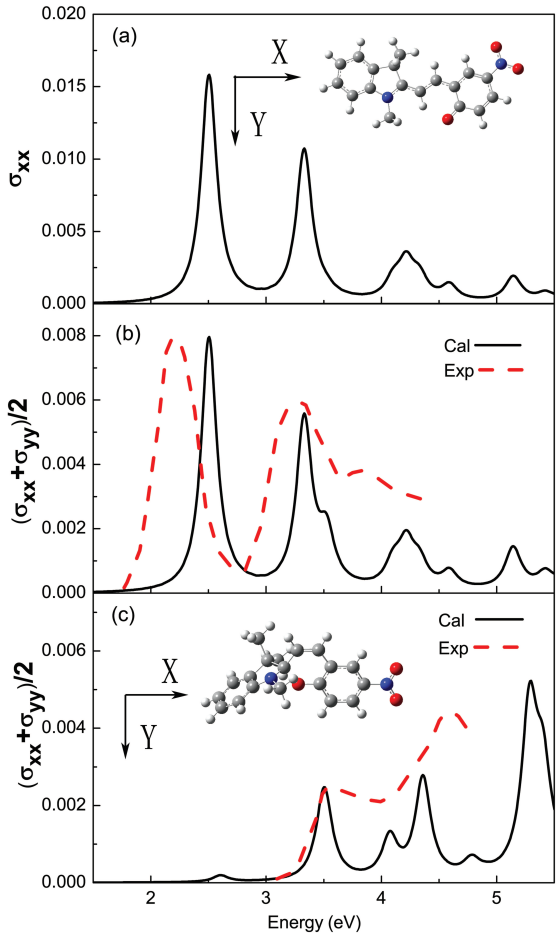

FIG. 4: The geometries and absorption cross sections of MC and SP molecules in gas phase. (a) σ_{xx} of MC molecule. (b)The average value of σ_{xx} and σ_{yy} of MC. (c)The average value of σ_{xx} and σ_{yy} of SP molecule.

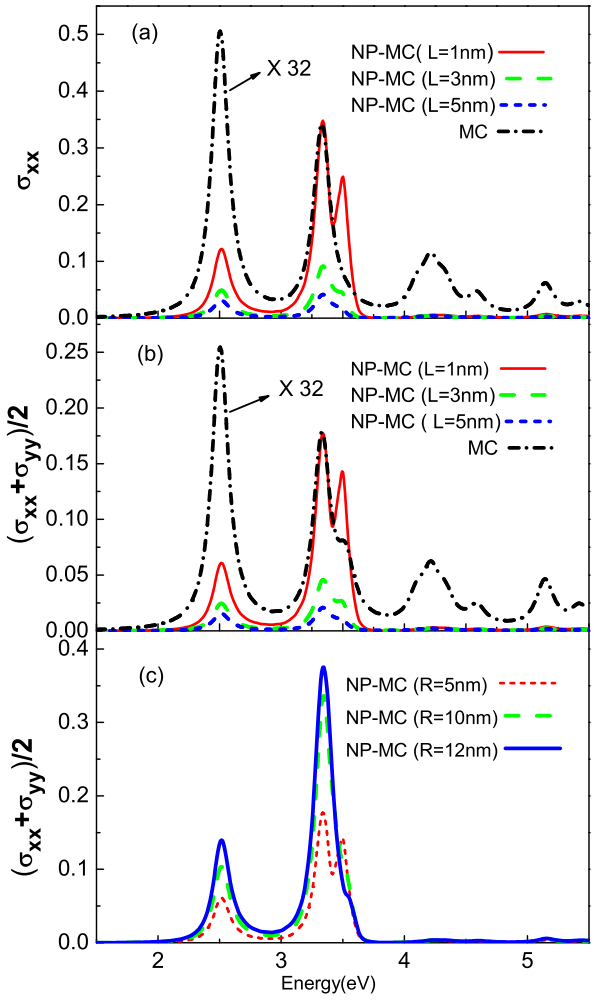

FIG. 5: (a) σ_{xx} of NP-MC system at $R = 5$ nm and $L = 1$, 3, 5 nm (the closest distance of MC mass center to NP surface along the x-axis). The absorption cross section of MC molecule is shown for the comparison, and its intensity is multiplied by 32. (b) The average absorption cross sections of NP-MC system at $R = 5$ nm and $L = 1$, 3, 5 nm. (c) The average absorption cross sections of NP-MC system at $L = 1$ nm and $R = 5$, 10 and 12 nm.

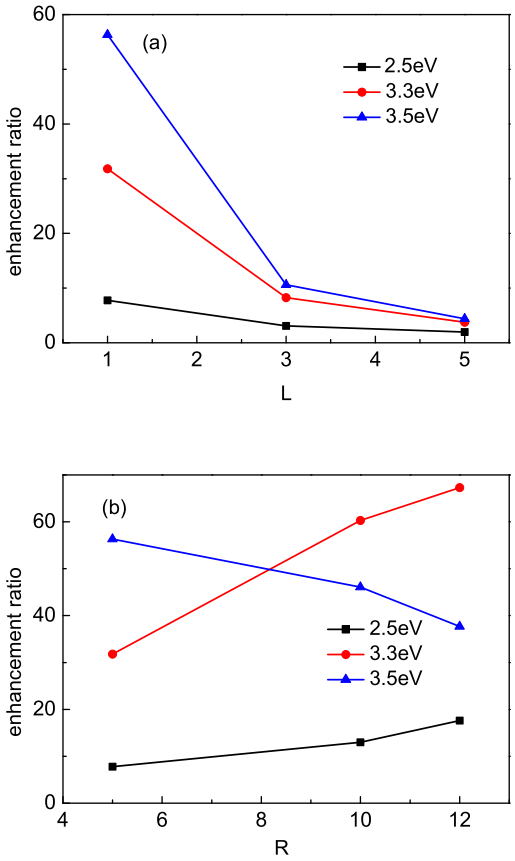

FIG. 6: (a)The variation of AERs for three low-energy absorption bands in the average absorption cross sections of NP-MC system vs L at $R = 5$ nm. (b)The variation of AERs vs R at $L = 1$ nm.

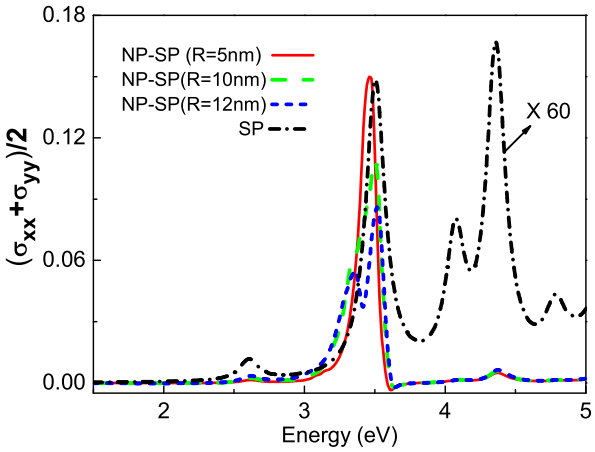

FIG. 7: The average absorption cross sections of the isolated SP molecule and the NP-SP system with different size Ag NPs. The absorption intensity of the isolated SP molecule is multiplied by 60.

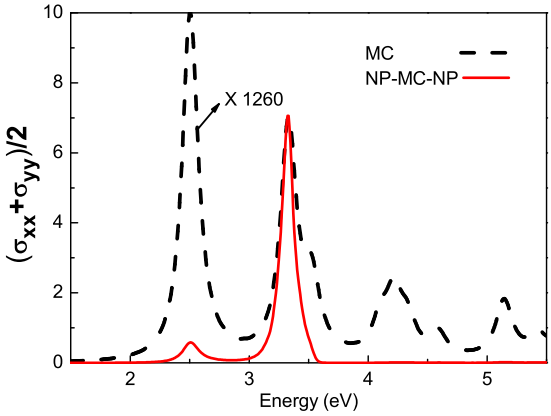

FIG. 8: Absorption spectra of NP-MC-NP system composed of two identical NPs and MC molecule. MC is set between two Ag NPs arranged along the $x-$axis. The average absorption cross section of the isolated MC molecule is also displayed and is multiplied by 1260.